Electronic Supplementary Material (ESI) for Physical Chemistry Chemical Physics.

Supporting Information: Pressure Increases the Ice-like Order of Water at Hydrophobic Interfaces

Christoph Hölzl and Dominik Horinek*

Institut für Physikalische und Theoretische Chemie, Universität Regensburg, 93040 Regensburg, Germany

E-mail: dominik.horinek@ur.de

Simulation Details

The simulations were performed with GROMACS 4.6.5.[1] Three-dimensional periodic boundary conditions were applied to the system. The system geometry is a rectangular box with sizes ranging from 3.036 x 2.629 x 10.1 nm^3 at 1 bar to 3.036 x 2.629 x 8.3 nm^3 at 10 kbar. The Lennard-Jones interactions between different atoms were calculated using the Lorentz-Berthelot combination rule. Lennard-Jones and real-space Coulomb interactions were cut off at 1 nm, and long range electrostatics were calculated using smooth PME[2] with a lattice spacing of 0.12 nm. The SETTLE[3] algorithm was used to constrain the water geometry, and LINCS[4] was used to keep all bond lengths involving hydrogen rigid. A time step of 1.5 fs was used. The temperature was controlled using stochastic velocity rescaling,[5] while the pressure component orthogonal to the interface was controlled using an anisotropic Berendsen barostat.[6] The hydrophobic interface was modeled to mimic a self-assembled monolayer (SAM) of octadecyltrichlorosilane on a silicon wafer as used in previous work.[7] The first carbon atoms of the 36 octadecane chains were placed on a hexagonal grid with a lattice constant of 5.06 Å and the chains were initially oriented in parallel. Besides the fixed positions of the first carbon atoms, no further constraints were placed on the alkane chains and they were allowed to move and arrange into a packed monolayer. The Lennard-Jones parameters of the AMBER03 force field[8] were used to describe the alkane chains. The small alkane charges of the OPLS-AA force field were used to account for the weak electrostatics of alkanes. For water the TIP4P/2005[9] model was used, which accurately reproduces the properties of water up to high pressures. The SAM-water interface was simulated for 210 ns at 300 K at seven pressures from 1 bar to 10 kbar. Additionally, the SAM-ice interface was simulated at 200 K and 1 bar for 120 ns. In order to fit the SAM and ice systems together the lattice constant of the fixed octadecane chains was changed to that of hexagonal ice (4.51 Å). The bulk ice systems were simulated using anisotropic pressure coupling. The ice Ih system with 432 water molecules was simulated at 200 K and 1 bar for 5 ns, and the ice VI system with 640 water molecules was simulated at 300 K and 25 kbar for 5 ns. The

SAM-water systems at 250, 350, and 400 K were simulated for 15 ns.

Water Orientations

In the probability distributions of the angles ξ and τ relative to the bulk phase, the bin size in z-direction was scaled with the compression of the box at the respective pressure. The bin sizes are 0.5 Å at 1 bar, 0.465 Å at 2 kbar, and 0.436 Å at 5 kbar. The three bins cover the z-ranges -0.100 – 0.050 nm at 1 bar, -0.093 – 0.047 nm at 2 kbar, and -0.087 – 0.044 nm at 5 kbar.

Coordination numbers

The coordination number of a water molecule was determined as the number of water molecules with an oxygen-oxygen distance from the central water smaller than the position of the first minimum of the radial distribution function of bulk water at 1 bar.

Hydrogen Bonding

For the definition of hydrogen bonds the geometric criterion by Imoto et al.[10] was used:

$$r_{\mathrm{H}\cdots\mathrm{O}} < -0.171\,\mathrm{nm} \cdot \cos\left(\alpha_{\mathrm{O}-\mathrm{H}\cdots\mathrm{O}}\right) + 0.137\,\mathrm{nm} \tag{1}$$

After calculating all hydrogen bonds in the system we detected rings in the hydrogen bond network and calculated the ring twist χ_{R} using the ring detection algorithm and ring twist definition by Matsumoto et al:[11,12]

$$\chi_{\mathrm{R}} = \left| \frac{1}{n} \sum_{i=0}^{n-1} \sin\left(3\theta_{ijkl}\right) \right| \tag{2}$$

Here n is the ring size, θ_{ijkl} is the torsional angle, and the water indices in a ring are $j = (i+1)$ mod n, $k = (i+2)$ mod n, and $l = (i+3)$ mod n. χ_{R} is 0 when all water molecules in the ring are tetrahedrally coordinated, e.g. in a chair or boat conformation for 6-rings, or when all water molecules are in a plane, or when the twists cancel each other out. Ring conformations deviating strongly from the tetrahedral case would however disturb the local H-bond network and are unlikely to occur. A ring is considered to be ice-like when its twist χ_{R} is below a cutoff χ_c, which is defined such that

$$\int_0^{\chi_c} P_{\mathrm{ice}}(\chi)\,\mathrm{d}\chi \geq 0.999 \tag{3}$$

where $P_{\mathrm{ice}}(\chi)$ is the twist distribution in a 0.5 Å slice of an ice layer from a bulk ice simulation (see the density profile in Figure 1 and the twist distribution in Figure 2) and $\chi_c = 6.5°$.

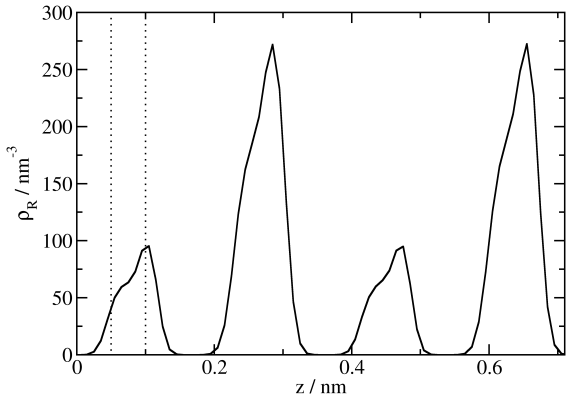

Figure 1: Laterally averaged 6-ring density profile in bulk ice Ih. The dotted lines are the 0.5 Å slice for which χ_c was determined. Since only the rings in chair conformation of a single ice layer orthogonal to the c-axis are of interest, the higher density peaks of rings in boat conformation between the layers are ignored for the determination of the ring twist in a single ice layer. The maximum ring density in an ice layer is then 95 nm^{-3}.

The excess of ice-like rings is then:

$$\rho_{\mathrm{R}}^{\mathrm{ex}}(z) = \rho_{\mathrm{R}}(z) \int_0^{\chi_c} \left[P(\chi_{\mathrm{R}}, z) - P_{\mathrm{bulk}}(\chi_{\mathrm{R}})\right] \mathrm{d}\chi_{\mathrm{R}} \tag{4}$$

We used the following ring detection algorithm, which is equivalent to the method used

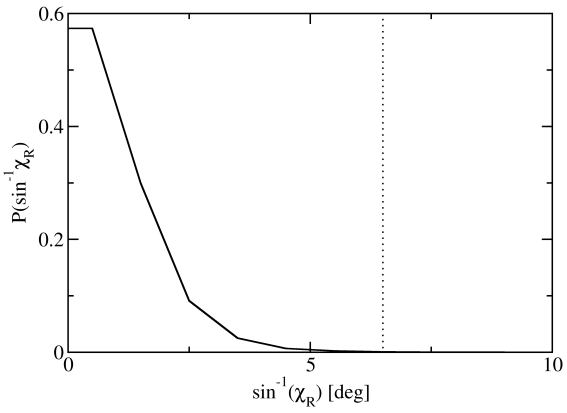

Figure 2: Ring twist distribution for a 0.5 Å slice of bulk ice. The dotted line is at $\sin^{-1}(\chi_c) = 6.5°$.

by Matsumoto et al.:[11] The H-bond network is represented as an undirected graph which has one vertex corresponding to each water molecule. Two vertices are connected by an edge if the corresponding water molecules are H-bonded. For each triplet of connected vertices (a, b, c) there exists a ring of size n if the shortest path from a to c which does not contain the vertex b (the vertex adjacent to both a and c) is of length $n-2$. Multiple rings exist for one triplet if more than one shortest path exists.

Temperature dependence of the interfacial properties

Figure 3 contains all the profiles analyzed in the main text for temperatures from 250 to 400 K.

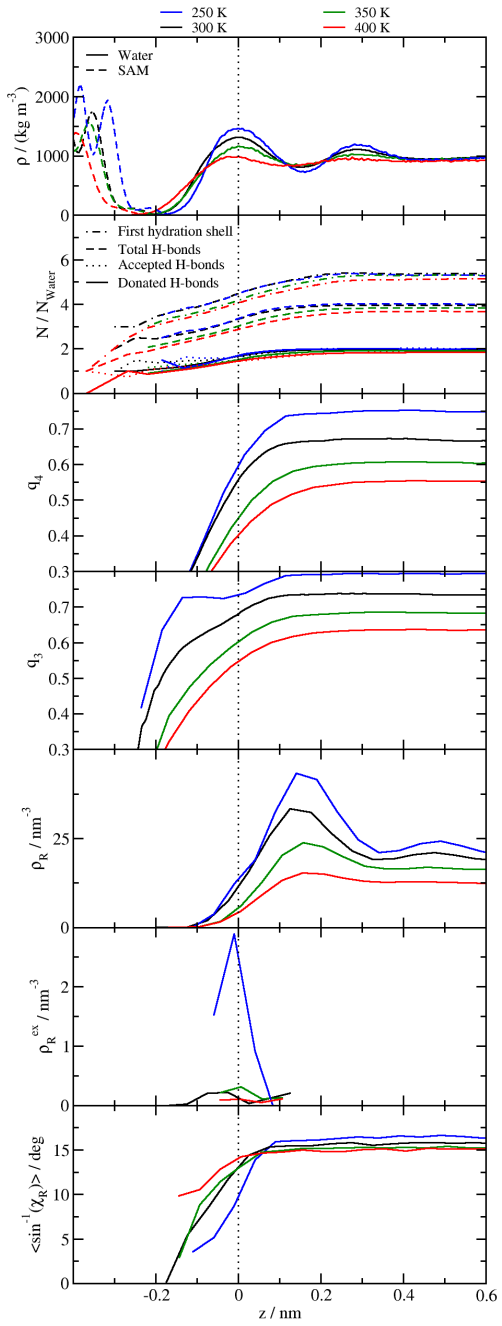

Figure 3: Laterally averaged profiles of the SAM-water interface at 1 bar for different Temperatures from 250 to 400 K.

Ring densities and twist of other ring sizes

The ring density on its own is not a measure of ice-likeness, as shown by the increase of the bulk ring densities of different sizes:

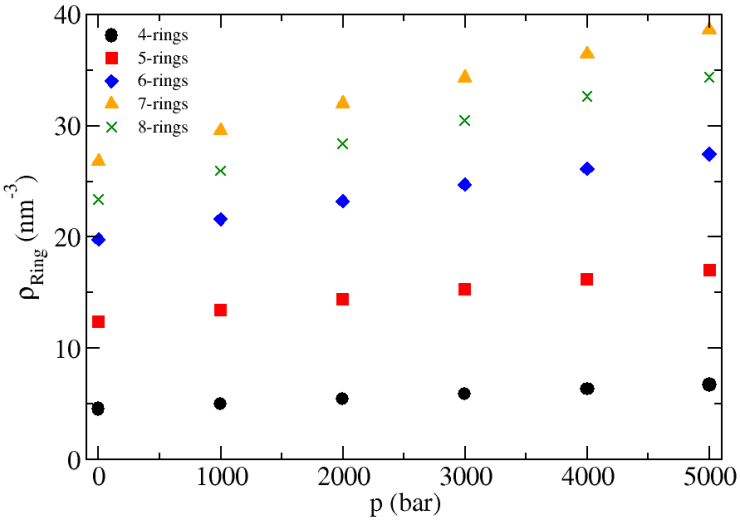

Figure 4: Bulk ring densities of four- to eight-membered rings at 300 K as a function of pressure.

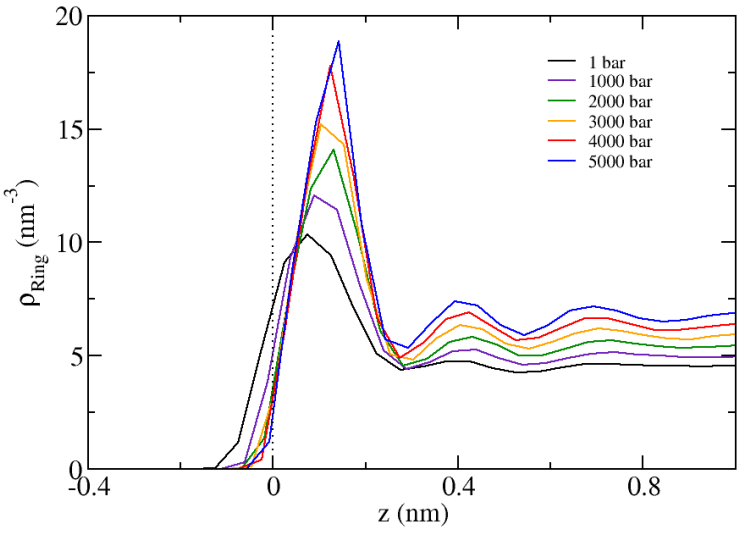

Figure 5: Density profiles of four-membered rings.

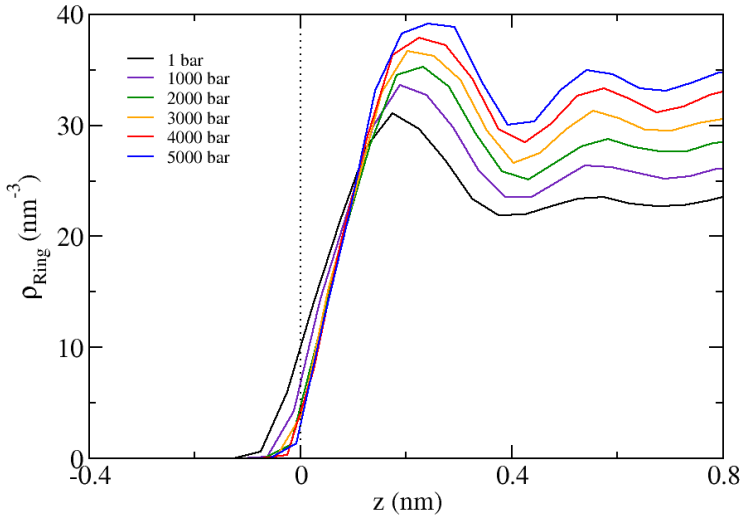

Figure 6: Density profiles of eight-membered rings.

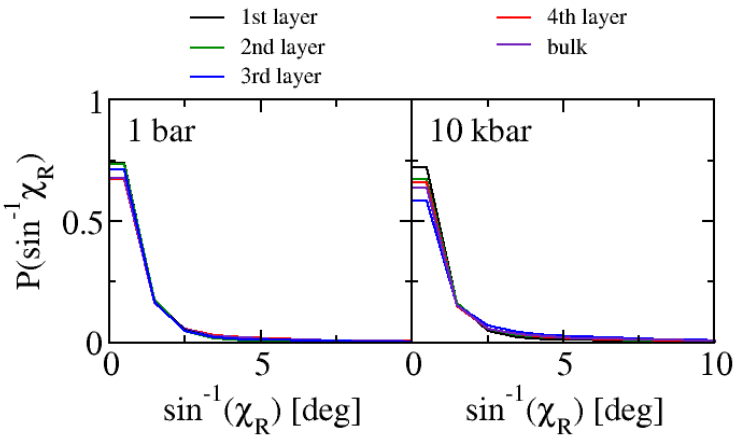

Figure 7: Ring twist of four-membered rings.

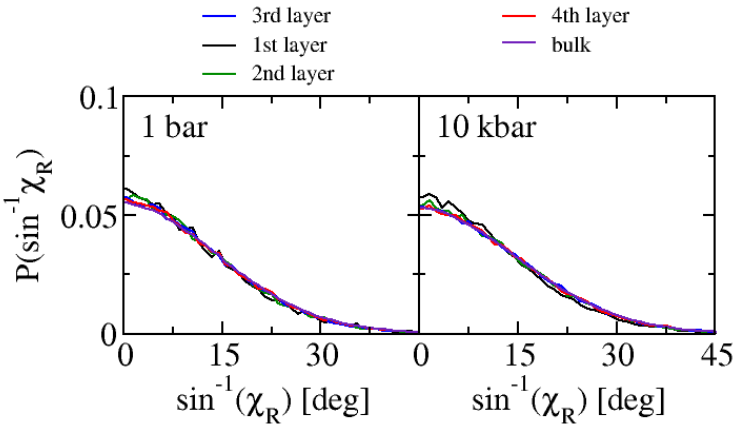

Figure 8: Ring twist of eight-membered rings.

Snapshots of the SAM/water system

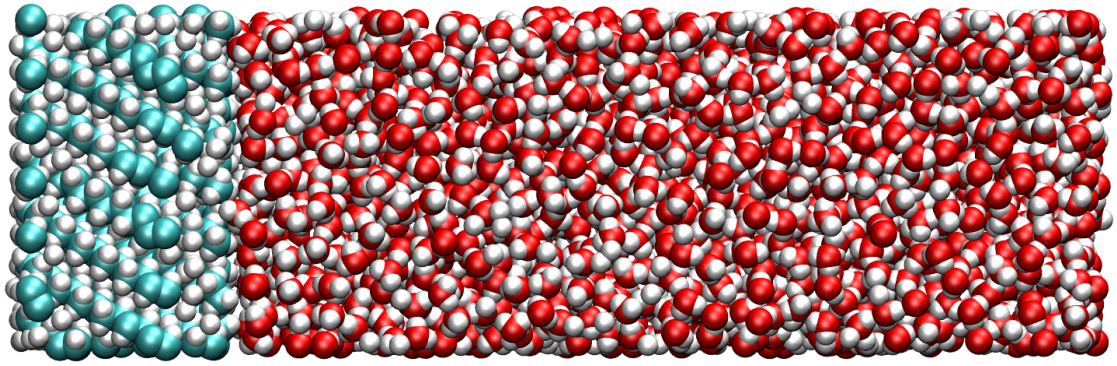

Figure 9: Snapshot of the full SAM/water system at 300 K and 1 bar. Hydrogen atoms are white, oxygen is red, and carbon is cyan. Images from periodic boundary conditions are not shown.

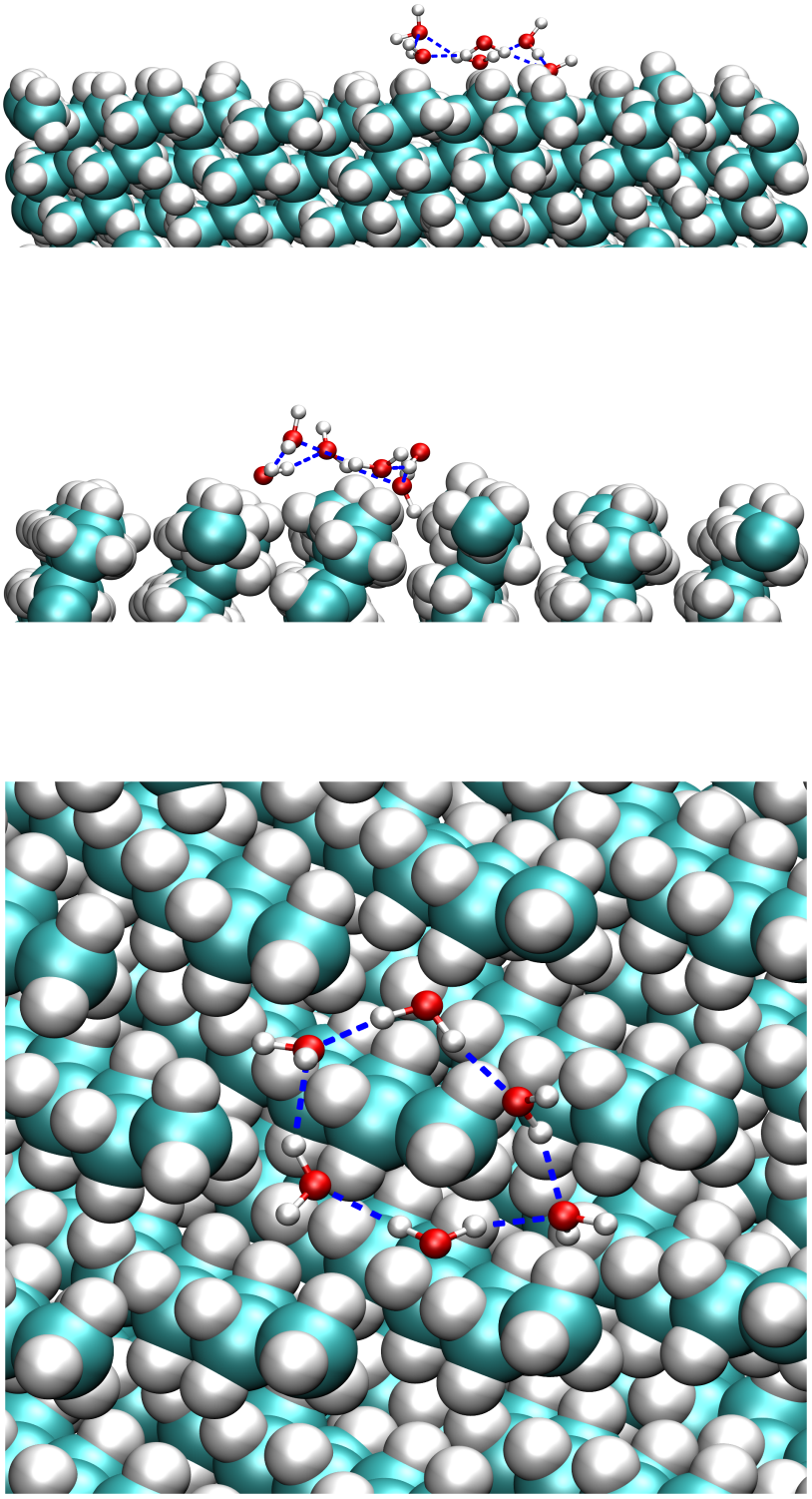

Figure 10: Snapshots of one ice-like ring at the interface at 300 K and 1 bar. Two side views and one top-down view. Hydrogen bonds are shown as blue dashed lines.

Ice VI

Bulk water transitions to ice VI at 300 K and about 10 kbar. This ice phase is also present in the phase diagram of the TIP4P/2005 water model, although the necessary pressure at 300 K is significantly higher at 25 kbar.[13] Figure 11 contains the ring density profiles from four- to ten-membered rings for a simulation at 25 kbar and an ideal crystal. The perfect crystal contains exclusively four- and eight-membered rings. Although the simulation results show some defects, the amount of six-membered rings is insignificant in ice VI.

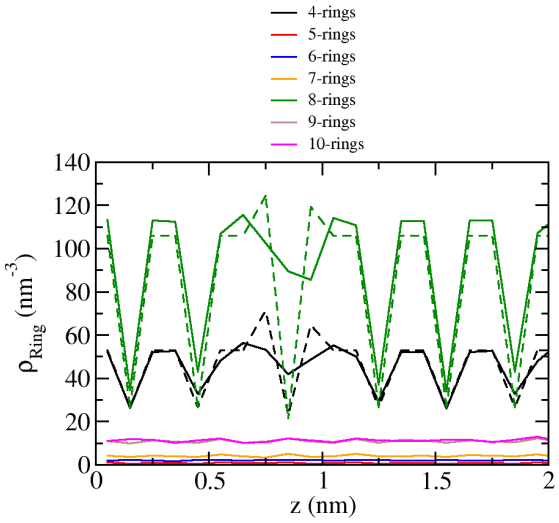

Figure 11: Laterally averaged ring density profiles in bulk ice VI. The full lines are the results of a simulation at 25 kbar using the TIP4P/2005 water model. The dashed lines are the analysis of a perfect ice crystal obtained from the `genice` program.[14] The same crystal was also used as the starting geometry for the simulation.

References

(1) Hess, B.; Kutzner, C.; van der Spoel, D.; Lindahl, E. GROMACS 4: Algorithms for Highly Efficient, Load-Balanced, and Scalable Molecular Simulation. *J. Chem. Theory Comput.* **2008**, *4*, 435.

(2) Essmann, U.; Perera, L.; Berkowitz, M. L.; Darden, T.; Lee, H.; Pedersen, L. G. A smooth particle mesh Ewald method. *J. Chem. Phys.* **1995**, *103*, 8577.

(3) Miyamoto, S.; Kollman, P. SETTLE: an analytical version of the SHAKE and RATTLE algorithm for rigid water models. *J. Comput. Chem.* **1992**, *13*, 952.

(4) Hess, B.; Bekker, H.; Berendsen, H. J. C.; Fraaije, J. G. E. M. LINCS: A Linear Constraint Solver for Molecular Simulations. *J. Comput. Chem.* **1997**, *18*, 1463.

(5) Bussi, G.; Donadio, D.; Parrinello, M. Canonical sampling through velocity rescaling. *J. Chem. Phys.* **2007**, *126*, 014101.

(6) Berendsen, H. J. C.; Postma, J. P. M.; van Gunsteren, W. F.; DiNola, A.; Haak, J. R. Molecular dynamics with coupling to an external bath. *J. Chem. Phys.* **1984**, *81*, 3684.

(7) Wirkert, F. J.; Hölzl, C.; Paulus, M.; Salmen, P.; Tolan, M.; Horinek, D.; Nase, J. The Hydrophobic Gap at High Hydrostatic Pressures. *Angew. Chem. Int. Ed.* **2017**, *56*, 12958.

(8) Duan, Y.; Wu, C.; Chowdhury, S.; Lee, M. C.; Xiong, G.; Zhang, W.; Yang, R.; Cieplak, P.; Luo, R.; Lee, T. et al. A Point-Charge Force Field for Molecular Mechanics Simulations of Proteins Based on Condensed-Phase Quantum Mechanical Calculations. *J. Comput. Chem.* **2003**, *24*, 1999.

(9) Abascal, J. L. F.; Vega, C. A general purpose model for the condensed phases of water: TIP4P/2005. *J. Chem. Phys.* **2005**, *123*, 234505.

(10) Imoto, S.; Forbert, H.; Marx, D. Water structure and solvation of osmolytes at high hydrostatic pressure: pure water and TMAO solutions at 10 kbar versus 1 bar. *Phys. Chem. Chem. Phys.* **2015**, *17*, 24224.

(11) Matsumoto, M.; Baba, A.; Ohmine, I. Topological building blocks of hydrogen bond network in water. *J. Chem. Phys.* **2007**, *127*, 134504.

(12) Matsumoto, M.; Yagasaki, T.; Tanaka, H. Chiral Ordering in Supercooled Liquid Water and Amorphous Ice. *Phys. Rev. Lett.* **2015**, *115*, 197801.

(13) Aragones, J. L.; Conde, M. M.; Noya, E. G.; Vega, C. The phase diagram of water at high pressures as obtained by computer simulations of the TIP4P/2005 model: The appearance of a plastic crystal phase. *Phys. Chem. Chem. Phys.* **2009**, *11*, 543.

(14) Matsumoto, M.; Yagasaki, T.; Tanaka, H. GenIce: Hydrogen-Disordered Ice Generator. *J. Comp. Chem.* **2018**, *39*, 61.